Solid Earth Discuss., 4, 1317–1344, 2012
www.solid-earth-discuss.net/4/1317/2012/
doi:10.5194/sed-4-1317-2012

Solid Earth
Discussions

Seismic imaging of sandbox experiments – laboratory hardware setup and first reflection seismic sections

C. M. Krawczyk[1,*], **M.-L. Buddensiek**[2,*], **O. Oncken**[3], **and N. Kukowski**[4,*]

[1]Leibniz-Institute for Applied Geophysics (LIAG), Stilleweg 2, 30655 Hannover, Germany
[2]SINTEF Petroleum Research, S. P. Andersens Veg 15, 7031 Trondheim, Norway
[3]Helmholtz-Centre Potsdam (GFZ), Telegrafenberg, 14473 Potsdam, Germany
[4]Friedrich Schiller University, Institute for Geosciences, Burgweg 11, 07749 Jena, Germany
[*]formerly at: GFZ Potsdam, Germany

Received: 2 August 2012 – Accepted: 3 August 2012 – Published: 10 October 2012

Correspondence to: C. M. Krawczyk (lotte@liag-hannover.de)

Published by Copernicus Publications on behalf of the European Geosciences Union.

Abstract

With the study and technical development introduced here, we combine analogue sandbox simulation techniques with seismic physical modelling of sandbox models. For that purpose, we designed and developed a new mini-seismic facility for laboratory use, comprising a seismic tank, a PC-driven control unit, a positioning system, and piezoelectric transducers used here the first time in an array mode. To assess the possibilities and limits of seismic imaging of small-scale structures in sandbox models, different geometry setups were tested in the first experiments that also tested the proper functioning of the device and studied the seismo-elastic properties of the granular media used. Simple two-layer models of different materials and layer thicknesses as well as a more complex model comprising channels and shear zones were tested using different acquisition geometries and signal properties. We suggest using well sorted and well rounded grains with little surface roughness (glass beads). Source receiver-offsets less than 14 cm for imaging structures as small as 2.0–1.5 mm size have proven feasible. This is the best compromise between wide beam and high energy output, and being applicable with a consistent waveform. Resolution of the interfaces of layers of granular materials depends on the interface preparation rather than on the material itself. Flat grading of interfaces and powder coverage yields the clearest interface reflections. Finally, sandbox seismic sections provide images of very good quality showing constant thickness layers as well as predefined channel structures and fault traces from shear zones. Since these can be regarded in sandbox models as zones of decompaction, they behave as reflectors and can be imaged. The multiple-offset surveying introduced here improves the quality with respect to S/N-ratio and source signature even more; the maximum depth penetration in glass bead layers thereby amounts to 5 cm. Thus, the presented mini-seismic device is already able to resolve structures within simple models of saturated porous media, so that multiple-offset seismic imaging of shallow sandbox models, that are structurally evolving, is generally feasible.

1 Introduction

There is a growing need of measuring active processes acting in the Earth's crust and their influence on the surface for both pure and applied research. Additionally, the rapidly evolving geodetic, geophysical and geological observation techniques increase the challenge to integrate all those techniques. Thus, to account for this development, seismic imaging and monitoring techniques have to be integrated, notably involving surface observations from e.g. satellites, in order to understand active deformation of structures relevant in the crust. This problem has not been fully or systematically approached, since material and logistic expenses are high with respect to field experiments.

In the laboratory, less expensive tools like analogue sandbox simulation have been applied to study geological processes (e.g., Davis et al. 1983; Storti et al., 2000; Lohrmann et al., 2003; Gartrell et al., 2005; Hoth et al., 2007, 2008; Boutelier and Oncken, 2011). Sandbox experiments offer unique insights into geodynamic processes, as they allow direct observation of processes, e.g. orogenic wedge evolution, fault activity, or lithospheric scale deformation, which are taking place in inaccessible depths and times. Most of the analogue materials representing upper crustal rocks and sediments, like the widely used quartz sand, corundum sand, mortar, or sugar, are opaque. Thus, direct observation of deformation is only possible at the surface of 3-D models or through bordering glass planes of 2-D models. Although recently new monitoring techniques like X-ray computer tomography (Coletta et al., 1991; Schreurs et al., 2003), particle image velocimetry (PIV, e.g. Baldassarre et al., 2001; Wolf et al., 2003; Hampel et al., 2004; Adam et al., 2005; Rosenau et al., 2009; Reiter et al., 2011), or laser scanning (e.g. Persson et al., 2004; Graveleau and Dominguez, 2008) have led to significant improvements in analysing and transfering sandbox experiments, the challenge to monitor 3-D evolution of structures within opaque bodies remains. To overcome this deficiency, seismic imaging of sandbox models is suggested to provide a promising tool.

Sherlock (1999) and Sherlock and Evans (2001) have shown that seismic imaging of structures in granular models is feasible. Because their seismic modelling of granular material is based on zero-offset data, the experiments suffered from high attenuation and especially scattering. Bodet et al. (2010) implemented a monitoring tool based on laser-Doppler vibrometry to systematically characterise granular material in analogue models. They analyzed P-wave first arrival times and surface-wave dispersion regarding the velocity structure. Results correlate well with dispersion relations for acoustic waves of Jacob et al. (2008) who used a mechanical source for the experiment. However, these attempts do not provide structural images but were restricted to providing good estimates of elastic material properties. This is in parts overcome by the laser interferometry setup provide by Bretaudeaux et al. (2011) who additionally applied finite element viscoelastic modelling to confirm time arrivals and amplitudes of experiments in thermoplastic and resin-based models.

We chose to develop an experimental setup with regard to advanced processing steps, the use of an array of receivers and the application of reflection processing to minimize noise (Krawczyk et al., 2007; Buddensiek, 2009). Since the small dilation between sand grains generated by shearing causes reflections, geologic models containing 2 to 3 layers of different densities and a few shearing structures are suitable for imaging. The requirements and sequential aims of such an experimental study encompass (1) a systematic approach to test the material properties and the effects of wave propagation in an-/isotropic media by physical studies (see Buddensiek et al., 2009); (2) various imaging and processing techniques to be tested first on static models, in order to reproduce scaled active seismic experiments (this study); and, finally, (3) time-lapse imaging of deforming 3-D structural models.

The main advantage of the application of a mini-seismic system is its non-invasiveness as opposed to the conventional method of slicing the analogue sandbox model, so that time-lapse monitoring can be applied. Even though X-ray computerized tomography (CT) analysis also allows the visualization of the interior of an analogue model without destroying it (Colletta et al., 1991; Schreurs et al., 2003), it still requires the analysis of distinct scenes of an evolving model sequence (see Holland et al., 2011). Here, we introduce the new laboratory facility and its technical specifications, and also discuss the tested geometry and material variations based on the first data generation produced by multiple-offset surveying.

2 Experimental setup and equipment development

The characteristics of the four major components of the mini-seismic system – seismic tank, control unit, positioning system, transducers – are summarised below. Technical specifications are given in Table 1, while Figs. 1 to 3 illustrate the new device and its components.

The requirements and use of technical components as well as the imaging requisites refer also to scaling factors defined by analogue experiments. Here, we consider the set-up tested by Lohrmann and co-workers (2003) followed by Adam and co-workers (2005) who used granular material that obeys Mohr-Coulomb rheology and scales to nature through its mechanical properties, i.e. friction and cohesion. Thereby, typical crustal materials and kinematic domains are simulated properly. Since 1 cm in the model scales to 1 km in nature, we want to test acquisition geometries in the lab on a tectonic scale first. Thus, our geometry simulates tectonic settings of up to 15 km horizontal distance, where fault segments of a 100 m width are present. This translates to 150 mm offset and mm-width of structures to be investigated by the mini-seismic device.

2.1 The seismic tank

The largest constituent of the laboratory seismic device is a plexiglass tank of 1 m × 1 m × 0.4 m dimension (Fig. 1), in which the experiments are conducted. The plexiglass tank is filled with layers of saturated sand resembling geological structures in question on a cm-scale following the needs of physically and geometrically correct scaling (e.g. Hubbert, 1937; Krantz, 1991; Lohrmann et al., 2003). For good coupling, the tank is filled with water after the model has been sieved in and saturated. Saturation time of three to four days was found to be well suited. The sample should be positioned in the centre of the tank to avoid strong side effects during data acquisition.

2.2 PC system with control unit

An industry PC (type IPC-9401) contains the signal generator including a signal amplifier and a transient recorder with pre-amplifier. The PC also drives the step motors for the positioning of the source and receivers (Fig. 2).

The technical parameters of the signal generator allow a broad bandwidth and frequency range of the emitted signals that can be recorded in different dynamic ranges (Table 1). Depending on the experiment, different waveforms are available for emission as source signal. This may either be a step function or could consist of 1–10 periods with frequencies between 0.05 to 1 kHz, including also additional tapering by sine and cosine envelopes of variable order. For recording of reflected signals, the transient recorder contains three boards with four channels each (Table 1). Thereby, the number of transducers in our laboratory seismic facility is limited to twelve. The channels can be actuated individually, with a memory of 2 Msamples/channel and maximum sampling of 20 MHz (14 bit).

2.3 Positioning system

Two step motors move the sensors along the horizontal axes (Fig. 1). They can move any given source and receiver geometry horizontally within the tank, so that seismic profiles can be recorded at any position over the model, resembling scaled 3-D marine survey geometries.

The maximum traverse path is 1 m depending on sensor configuration. With an accuracy of 0.12 mm/motor step it is possible to move an array to any defined position sufficiently precise (Table 1).

2.4 Transducers

Piezo-electric transducers that are lowered into the tank are used as ultrasound source and receivers (Fig. 3). They can be assembled with a rack design of any geometry. So far, twelve receivers and one emitter (custom-made product) with piezo-electric converters are in use.

Coated by a damped brass cylinder of 12 mm diameter and 20 mm hight, the lead-methaniobate piezo-electric element contained is 2 mm high with 5 mm diameter. It is glued to a thin brass plate, so that internal reflections are negligible. The performance of the piezo-electric transducers has been extensively tested (see Buddensiek et al., 2009), showing maximum sensitivity at 425 kHz with half-power bandwidth between 250–675 kHz (see Fig. 3, Table 1). After analysing effective diameter of the transducers, directionality, changes in waveform, and frequency sensitivity, Buddensiek et al. (2009) recommend to use signal frequencies of 350 to 550 kHz, with incidence angles below 35° and source receiver-offsets less than 14 cm in order to exploit the piezo-electric transducers in an optimal way. This finally allows the imaging of structures as small as 2.0–1.5 mm size.

3 Test experiments

The maximum source frequency of 1 MHz allows for a very high resolution in the mm-range, depending on the velocity of the material. However, if the resolution is close to the grain size, the grains cause scattering effects and attenuation, so that the S/N ratio is impaired. With one source and 12 simultaneously recording receivers we have therefore performed test and calibration experiments to decide about model preparation and to work out sufficient imaging quality. The acquisition geometry is based on 18 to 150 mm shot-receiver spacing, 12 mm receiver spacing, 3 mm shot spacing and 100 mm water depth. This design is adapted to resolve faults and other structures of a few mm width, as they are to be expected in sandbox models. The source specifications and processing parameters varied and are given accordingly in the following subchapters.

3.1 Principle geometries

In order to determine the possibilities and limits of our apparatus to image geological structures, the first experiments are kept very simple. 2-layer models with layers composed of different materials (water-saturated sand of different grain sizes and resin-saturated sand) or different material densities are acquired testing also variable layer thicknesses and different source frequencies (Fig. 4). For all experiments presented here, a sinusoid source wavelet of four periods tapered by a squared cosine, 16-fold vertical stacking, and a sampling rate of 20 MHz have been applied.

A first experiment series acquired data across a flat lying, 4.5 cm thick concrete body embedded in sand (Fig. 4a, b). Here, the source frequency varied systematically between 100 kHz and 1 MHz. The results show that resolution and attenuation are much higher using a 1 MHz source frequency than is observed in the 175 kHz experiment. Enough energy passes through the sand to be reflected at the bottom of the seismic tank, whereas no bottom reflection can be seen underneath the concrete-water interface due to the higher attenuation for high frequencies (Fig. 4a, b).

The next experiments acquired data across a wedge-shaped body, consisting of either concrete in sand (Fig. 4c) or a layer of glass beads beneath a sand wedge (Fig. 4d). For both experiments the source frequency was 700 kHz. Reflections from the top of the concrete can be seen for up to 4.5 cm of sand layer thickness, when attenuation becomes too high for the high-frequency P-waves (Fig. 4c). For the glass-bead setup, the resulting seismogram shows significant noise due to scattering, so that no clear reflection of the sand-glass bead interface is visible. However, the glass bead layer contains less scattering noise than the sand layer due to the longer wavelength of the P-wave signal. Despite this, the artificially introduced shear zone in the top third of the wedge can be depicted more clearly (Fig. 4d).

Additionally, first parameter tests show that models with sand grains <0.4 mm and a source frequency of 250 kHz produce a reasonably good data quality. Furthermore, reflections of an interface between uncompacted sand with grain size <0.6 mm and denser, compacted sand (grain size <0.4 mm) can be picked in the seismic sections using a source frequency of 350 kHz.

3.2 Interface preparation

We performed a second series of experiments in order to determine which model setup could create the strongest interface reflections. The interface model is a two-layer model that consists of four different granular materials, combined with four different procedures of interface preparation, so that 16 fields of interface variations can be analysed (Fig. 5). Layer thickness is constant at 2 cm, and the fields are 10 cm × 10 cm in size. Interface preparation either consisted of grading flat by soft stamping, of sprinkling with glass powder (40 to 70 µm diameter), of applying both, or none of them (for more detail see Buddensiek, 2009). Four profile locations cover the four different material interfaces, while the preparation types are surveyed inline (Fig. 5).

After a saturation time of three days, the seismic profiles were surveyed. For all sections presented here, a sinusoid source wavelet of four periods tapered by a squared cosine, 16-fold vertical stacking, and a sampling rate of 20 MHz have been applied. For seismic processing we only used the 450 kHz source frequency shots recorded at 18 mm offset, the nearest shot-receiver distance. Due to data acquisition very near to the model surface, only this trace provided enough sensitivity and a clear signal. Therefore, processing was kept simple by filtering only with an automatic gain control (AGC) of 0.04 µs window size.

From top to bottom, Fig. 6 reveals very different imaging results in the 16 fields of analysis (cf. Fig. 5). In all profiles both the surface of the model as well as the plexiglass bottom are easily identified as model boundaries. The ringing below the plexiglass reflections is dominant in profiles P1 and P2, while attenuation and scattering are higher in profiles P3 and P4 (Fig. 6). This directly relates with the material properties of either glass beads or sand, and with very high internal noise encountered in quartz and garnet sand, thereby hampering almost any reflection identification on profiles P3 and P4. Even the plexiglass bottom almost vanishes against the strongly pronounced multiple.

Glass beads of the same size constitute the layers of profile P1 (Fig. 6, P1). The interface, expected at ca. 0.09–0.1 µs, is faintly imaged where it had been prepared by powdering and grading plus powdering. The other panels with no preparation or grading only do not reveal clear reflectors. This observation also holds for profile P2, where reflections of the interface are strongest, because here glass beads of different size represent different layer properties. The upper layer shows only little noise, whereas the lower layer in profile P2 is more obscured, presumably by the diffractions generated at the interface that also affect the plexiglass signal (Fig. 6, P2). Profiles P3 and P4 yield a completely incoherent signal quality and, if any, only strongly discontinuous reflectivity, which could be expected for sands. Here, only internal scattering and noise occur, and the upper quartz sand layer already consumes the entire wave energy. Solely the water bottom multiple remains visible (Fig. 6, P3 and P4). Slope variations at the left side of the sections result from a collapse of the model boundary during the saturation phase prior to the seismic experiment.

In summary, the interface model experiment series suggests that grading flat plus powdering is the best suited procedure for interface preparation, which seems to be more important for a good imaging than the material itself. Furthermore, the use of well-rounded and well-sorted material (glass beads) is recommended. Three days saturation time should be sufficient in most cases.

4 Reflection seismic imaging

This advanced experiment series finally aimed at imaging different structural features by reflection seismic profiling across a 3-D model. The channel model has two layers of glass beads of different size, with their interface being prepared by flattening and powdering (Fig. 7). This procedure and the material used were chosen accordingly to the results gained from the second experiment series (see above). The channel model is 5 cm thick. It contains three distributed, 1 cm deep channels, and a 30°-dipping shear band created by pulling a string through the model after saturation of three days (cf. Buddensiek 2009 for experimental details). The resulting dilation and decompaction may be considered equivalent to that known to occur in natural fault zones and their process zone. Three seismic profiles were shot across the different channel locations and the shear zone (Fig. 7).

The acquisition geometry with 12 receivers was kept to 18–150 mm shot-receiver spacing, 3 mm shot spacing and 100 mm water depth. The source frequency was varied from 300 to 650 kHz, with 50 kHz intervals for individual frequency stacks of 256 vertical fold. For signal recording a sampling interval of 0.05 µs was chosen. The reflection seismic processing sequence comprised frequency stacking, spherical gain application, bandpass filtering (75, 125, 750, 800 kHz), normal move-out (NMO) correction (1485 m s^{-1} constant velocity), stacking and time-migration ($t-k$ domain).

With good quality, the three reflection seismic profiles across the channel model all image the predefined structures (Fig. 8, profiles a to c). The common-offset gathers reveal the pre-processed data quality, where diffraction hyperbolas occur at the surface outcrop of the shear band, thereby blurring the layer below (e.g., Fig. 8, left, profile a: 8-12 cm distance, 0.12–0.14 µs). As one would expect, largest diffractions are encountered from the flanks of the channel structure (e.g., Fig. 8, left, profile b: 25–30 cm distance, 0.15 µs), but also a number of small amplitude diffractions were generated at the layer interface (Fig. 8 left, all profiles: below 0.15 µs). Thus, the lower layer of the model appears noisier than the upper one. The model surface runs continuously across the sections, while the plexiglass bottom reveals a different amplitude behaviour in spite of a continuous reflection. It has a strong reflection where the interface is weak, and vice versa.

The migrated sections disclose the advantage of the multi-fold acquisition after NMO stacking. The diffractions described above are collapsed and the channel geometries are well defined (Fig. 8 right, all profiles: below 0.14 µs). Even the shear band is much better revealed from the surface down to at least the interface (Fig. 8 right, all profiles: 0.12 to 0.14 µs). The shear zone images by disruptions of the very strong bounding reflectors in the upper part. This effect is comparable to observations in the field across different scales (e.g., Krawczyk et al., 2002; 2006 and references therein). In addition, the shear zone can be further traced as smeared type of reflection zone down to the interface (best pronounced in Fig. 8b, right panel). Between the interface and the plexiglass bottom, however, the shear zone signal diminishes. This may be caused by the lower impedance contrast across the shear band if compared to the energy reflected at the layer interface.

After time-migration, the measured travel-time values and the known thicknesses from model preparation allow to check the consistency of our measurements. Picking the two-way travel-times from model surface, interface and plexiglass bottom, these layers are found on average at 0.12 µs, 0.144 µs and 0.187 µs. Calculating with a velocity value of 1485 m/s in the water column, the depth between transducers and model surface amounts to 9 cm, which is exactly the geometry used. The thickness of the upper model layer is 2 cm plus 1 cm where a channel is met. Assuming a velocity of 1600 m s^{-1}, the two-way travel-times of 0.024 µs and 0.012 µs fit very well. Inconsistencies in the thickness of the bottom layer may reach a few mm, if both model layers have the same velocity, which may be caused by imprecise sieving during model preparation or by incomplete velocities during migration.

Hence, the channel model has proven that variable layer thicknesses as well as shear bands are detected by seismic imaging of analogue models. Even though the fault is most clearly visible in the upper part of the top layer, it can also be imaged after stacking and migration in the deeper parts of the glass bead layers. With our hardware setup the penetration depth of this experiment is approximately 5 cm.

5 Discussion

The seismic sections of the interface model (Fig. 6) and channel model (Fig. 8) clearly showed that seismic surveys across glass bead models are more promising to produce clear reflections of interfaces, if these are carefully prepared and an array-technique is applied. The downside of models containing interfaces is that a substantial part of the energy is reflected. Thus, the energy-output of our source achieves a penetration depth of approximately 5 cm, which could not be improved by additional vertical stacking. None of the experiments was able to image an interface within sand. Since, in nature, most structural geologic information is achieved by imaging interfaces, and faults are usually inferred from horizon offsets, future experimental setups and experiments will have to focus on the interface preparation aspect for comparability with geometries observed in nature. Moreover, the current restriction in depth penetration will require the development of stronger sources while maintaining the frequency spectrum. Because of the required resolution of 1 to 3 mm, the source frequency cannot be lowered to achieve a higher penetration. However, if it is desired to perform multiple-offset processing, the source should, at the same time, emit a broad beam in the same frequency range.

Unlike field surveys, the seismic sections of the channel model (Fig. 8) showed that the decompaction due to shearing is imaged as a reflector itself. This shear band can be traced well down to 2.5 cm depth within sand, while the seismic expression of the shear band in glass beads is much smaller. The difference between both sections lies mostly in the material. Sand has a rougher surface, i.e. higher friction. Therefore, the grains are prone to stay in their displaced position after the string was pulled through. The smooth glass beads are more likely to fall back into place, so that the decompaction is not a permanent expression. In this case, not even less attenuation or a stronger source would enable us to resolve the shear zone. Nevertheless, seismic imaging is able to locate zones of decompaction within models that have undergone deformation. Ring shear testing of granular materials undergoing deformation first observe compaction before localized decompaction occurs along the zone of failure (Lohrmann et al., 2003). Therefore, the density contrast of shear zones versus undeformed material is even higher, and should be resolved even better in actively deforming models than in this simple simulation. If interfaces are present, the faults and their offset can be seismically imaged in glass bead models down to 2 cm. If additional interfaces are present below the depth-resolution for faults, the faults and their offset can be inferred from horizon offsets. In sand models, only the faults are well-resolved, but not the interfaces that are needed to infer an associated offset.

The seismic sections of the interface model (Fig. 6) show that the image quality over the glass bead profiles (P1 and P2) is much better than over the sand profiles (P3 and P4). A bigger 3-D model composed of sand would contain even more internal noise and attenuation. Since it is difficult to saturate sand models due to the rough surface of the grains, the imaging quality is variable from model to model and within one model. This result shows that sand, or any other granular material with a rough surface, is not suitable for seismic imaging with the preparation and saturation method that we use.

The discussion of the grain surface texture indicates a conflict of interest: A rough surface of the grains, i.e. higher friction, (1) creates proper shear bands that can be resolved in the seismic data, but (2) inhibits the saturation, which causes attenuation and noise. To avoid this conflict, the saturation needs to be improved. We used hot water of ca. 50° C to saturate, and waited for three days until the signal did not undergo further change. Further saturation can be achieved by a vacuum chamber, vibrations, a longer saturation time, and/or saturation with near boiling hot water. A vacuum chamber is not available for a setup of this size and vibration cannot be used, since it disturbs the packing, particularly at an interface. If the saturation time is supposed to take more than four days, we recommend using distilled water because of algae and other organic growth. In addition, the use of a low viscosity fluid with lower surface tension and wetting angle in contact to glass beads or sand may help to improve imaging quality.

Despite the limitations encountered during our experiments, recording multiple-offset traces and reflection processing was able to improve the image quality, also in comparison to Sherlock (1999) and Sherlock and Evans (2001), whose seismic modelling of granular material based on zero-offset data suffered from high attenuation and especially scattering. These imaging capabilities also supplement the vibrometry method of Bodet et al. (2010) that allows the derivation of elastic properties only. Since we are able now to resolve the interfaces within glass bead models, we can interpret faults in laboratory data like in field data.

6 Conclusions and outlook

We have designed and developed a new mini-seismic facility for laboratory use. It consists of a seismic tank, a PC control unit, a positioning system and includes piezo-electric transducers. First experiments with this setup have shown that ultrasonic seismic experiments are able to resolve structures within simple models of saturated porous media. The analysis of the seismic response as a function of layer thickness, material density contrast, and source frequency supports the design of future sandbox models to resolve specific structures systematically. Here, we suggest to use well sorted and well rounded grains with little surface roughness (glass beads), and to prepare the interfaces by grading and powdering to achieve a good imaging quality.

The acquisition and processing scheme that takes advantage of the redundant information provided by an array of receivers has proven successful here for more geological models. With the array-technique of piezo-electric transducers introduced here, we found the best compromise between wide beam and high energy output, the technique being applicable up to 14 cm offset with a consistent waveform. This enables imaging of structures as small as 2.0–1.5 mm size.

Seismic reflection imaging of different saturated analogue models detects layering and shear bands. Fault images can be resolved also in glass bead layering with increasing amplitude to larger depth. The multiple-offset surveying improves the data quality with respect to the S/N-ratio and allows for further processing steps, such that a depth penetration in glass bead layers of up to 5 cm is reached.

With respect to model and hardware setup, further developments should encompass the improvement of model saturation, the use of viscous material to simulate mantle material or salt domes, and the design of smaller sources with higher energy output and perfect signal control. Especially for more complex models, the image clarity and penetration depth need to be improved (setup of thin layer models) to study actively evolving models with this method. In the future, differences in wave propagation between field experiments and our laboratory system must be investigated to be able to compare both data records. However, the experiments show that multiple-offset seismic imaging of shallow sandbox models, that are structurally evolving, is generally feasible.

Acknowledgements. We thank Günter Tauscher and Thomas Ziegenhagen for their technical assistance in the laboratory, GMuG mbH, Bad Nauheim for technical support and sharing the codes, as well as Don Sherlock and Silvan Hoth for discussion. This study was funded by the GFZ Potsdam.

References

Adam, J., Urai, J. L., Wieneke, B., Oncken, O., Pfeiffer, K., Kukowski, N., Lohrmann, J., Hoth, S., van der Zee, W. and Schmatz, J.: Shear localisation and strain distribution during tectonic faulting – new insights from granular-flow experiments and high resolution optical image correlation techniques, J. Struct. Geol., 27, 283–301, 2005.

Adam, J., Schreurs, G., Klinkmüller, M., and Wieneke, S.: 2D/3-D Strain localisation and fault simulation in analogue experiments: insights from X-ray computed tomography and tomographic image correlation, Bolletino di Geofisica 49, 21–22, 2008.

Baldassarre, A., DeLucia, M., Nesi, P., and Rossi, F.: A Vision-Based Particle Tracking Velocimetry, Real-Time Imaging 7, 145–158, 2001.

Bodet, L., Jacob, X., Tournat, V., Mourgues, R. and Gusev, V.: Elasticity profile of an unconsolidated granular medium inferred from guided waves: Toward acoustic monitoring of analogue models, Tectonophysics, 496, 99–104, doi:10.1016/j.tecto.2010.10.004, 2010.

Boutelier, D. and Oncken, O.: 3-D thermo-mechanical laboratory modeling of plate-tectonics: modeling scheme, technique and first experiments, Solid Earth, 2, 35–51, doi:10.5194/se-2-35-2011, 2011.

Bretaudeau, F., Leparoux, D., Durand, O., and Abraham, O.: Small-scale modeling of onshore seismic experiment: A tool to validate numerical modeling and seismic imaging methods, Geophysics, 76, T101–T112, doi:10.1190/GEO2010-0339.1, 2011.

Buddensiek, M.-L.: Seismic imaging of sandbox models, PhD-Thesis, FU Berlin, http://www.diss.fu-berlin.de/diss/receive/FUDISS_thesis_000000009439, 2009.

Buddensiek, M.-L., Krawczyk, C. M., Kukowski, N., and Oncken, O.: Performance of piezo-crystal transducers with respect to amplitudes and waveform in laboratory seismic application, Geophysics, 74, T33–T45, 2009.

Colletta, B., Letouzey, J., Pinedo, R., Ballard, J. F., and Bale, P.: Computerized X-ray tomography analysis of sandbox models: examples from thin skinned thrust systems, Geology, 19, 1063–1067, 1991.

Davis, D., Suppe, J., and Dahlen, F. A.: Mechanics of fold-and-thrust belts and accretionary wedges, J. Geophys. Res., 88, 1153–1172, 1983.

Gartrell, A., Hudson, C., and Evans, B.: The influence of basement faults during extension and oblique inversion of the Makassar Straits rift system: Insights from analog models, AAPG Bulletin, 89, 495–506, doi:10.1306/12010404018, 2005.

Graveleau, F. and Dominguez, S.: Analogue modelling of the interaction between tectonics, erosion and sedimentation in foreland thrust belts, C.R. Geoscience, 340, 324–333, 2008.

Hampel, A., Adam, J., and Kukowski, N.: Response of the tectonically erosive South Peruvian forearc to subduction of the Nazca ridge: analysis of 3-D analogue experiments, Tectonics, 23, TC5003, doi:10.1029/2003TC001585, 2004.

Holland, M., van Gent, H., Bazalgette, L., Yassir, N., Hoogerduijn Strating, E. H., and Urai, J. L.: Evolution of dilatant fracture networks in a normal fault – Evidence from 4D model experiments, Earth Planet. Sci. Lett., 304, 399–406, doi:10.1016/j.epsl.2011.02.017, 2011.

Hoth, S., Hoffmann-Rothe, A., and Kukowski, N.: Frontal accretion: An internal clock for bivergent wedge deformation and surface uplift, J. Geophys. Res., 112, B06408, doi:10.1029/2006JB004357, 2007.

Hoth, S., Kukowski, N. and Oncken, O.: Distant effects in bivergent orogenic belts – How retro-wedge erosion triggers resource formation in pro-foreland basins, Earth Planet. Sci. Lett., 273, 28–37, doi:10.1016/j.epsl.2008.05.033, 2008.

Hubbert, M. K.: Theory of scale models as applied to the study of geological structures, Geol. Soc. Am. Bull., 48, 1459–1520, 1937.

Jacob, X., Aleshin, V., Tournat, V., Leclaire, P., Lauriks, W., and Gusev, V. E.: Acoustic Probing of the Jamming Transition in an Unconsolidated Granular Medium, Phys. Rev. Lett., 100, 158003, doi:10.1103/PhysRevLett.100.158003, 2008.

Krantz, R. W.: Measurement of friction coefficients and cohesion for faulting and fault reactivation in laboratory models using sand and sand mixtures, Tectonophysics 188, 203–207, 1991.

Krautkraemer, J. and Krautkraemer, H.: Werkstoffprüfung mit Ultraschall, Springer Verlag, Berlin, 1986.

Krawczyk, C. M., Eilts, F., Lassen, A., and Thybo, H.: Seismic evidence of Caledonian deformed crust and uppermost mantle structures in the northern part of the Trans-European Suture Zone (TESZ), SW Baltic Sea, Tectonophysics, 360, 215–244, 2002.

Krawczyk, C. M., Mechie, J., Lueth, S., Tasarova, Z., Wigger, P., Stiller, M., Brasse, H., Echtler, H. P., Araneda, M., and Bataille, K.: Geophysical Signatures and active tectonics at the South-Central Chilean margin, Front. Earth Sci., 1, 171–192, 2006.

Krawczyk, C. M., Buddensiek, M.-L., Philipp, J., Kukowski, N., and Oncken, O.: Midget seismic in sandbox models – hardware setup and first data generation. EAGE extended abstracts, E042, 5 pp., http://www.earthdoc.org/detail.php?pubid=6643, 2007.

Lohrmann, J., Kukowski, N., Adam, J., and Oncken, O.: The impact of analogue material properties on the geometry, kinematics, and dynamics of convergent sand wedges, J. Struct. Geol., 25, 1691–1711, 2003.

Persson, K. S., Garcia-Castellanos, D., and Sokoutis, D.: River transport effects on compressional belts: First results from an integrated analogue-numerical model, J. Geophys. Res., 109, B01409, doi:10.1029/2002JB002274, 2004.

Reiter, K., Kukowski, N., and Ratschbacher, L.: The interaction of two indenters in analogue experiments and implications for curved fold-and-thrust belts, Earth Planet. Sci. Lett., 302, 132–146, doi:10.1016/j.epsl.2010.12.002, 2011.

Rosenau, M., Nerlich, R., Brune, S., and Oncken, O.: Experimental insights into the scaling and variability of local tsunamis triggered by giant subduction megathrust earthquakes, J. Geophys. Res., 115, B09314, doi:10.1029/2009JB007100, 2010.

Schreurs, G., Hänni, R., Panien, M., and Vock, P.: Analysis of analogue models by helical X-ray computed tomography, Geol. Soc. Spec. Publ., 215, 213–223, 2003.

Sherlock, D. H.: Seismic imaging of sandbox models. PhD thesis, Curtin University, Perth, http://www.geophysics.curtin.edu.au/EGPPUBS/Docs/2000-000909-TPH.PDF, 1999.

Sherlock, D. H. and Evans, B. J.: The development of seismic reflection sandbox modelling, AAPG Bulletin, 85, 1645–1659, 2001.

Storti, F., Salvini, F., and McClay, K. R.: Synchronous and velocity-partitioned thrusting and thrust polarity reversal in experimentally produced, doubly-vergent thrust wedges – implications for natural orogens, Tectonics, 19, 378–396, 2000.

Wolf, H., König, D., and Triantafyllidis, T.: Experimental investigation of shear band patterns in granular material, J. Struct. Geol. 25, 1229–1240, 2003.

Table 1. Components and technical specifications of the laboratory seismic device.

Component	Partition	Technical specification
Seismic tank	aluminium table with plexiglass tray	size 1 m × 1 m × 0.4 m
PC control unit	signal generator (PCI-board, type MI6030)	max. output 125 MHz (14 bit); max. 8 Msamples; max. output amplitude ± 3 V
	signal amplifier (AC voltage signal amplifier)	input –2 to +2 V; input resistor 200 Ohm; output –141 to +141 V; output resistance 2 kOhm; bandwidth 20–500 kHz (–3 dB), 20–1000 kHz (–6 dB)
	pre-amplifier (type VV30)	30 dB voltage amplification and impedance tuning; frequency range 1 kHz–2 MHz; max. output amplitude ± 3 V
	transient recorder (three 4-channel PCI-boards, type MI4022)	for each channel signal amplifier and AD-converter; max. sampling 20 MHz (14 bit); max. memory 2 Msamples/channel
Positioning system	step motors	max. traverse path 1000 mm; accuracy 0.12 mm/motor step
Transducer	piezo-electric converters (leadmethaniobate)	max. sensitivity 425 kHz; size 5 mm diameter, 2 mm height; coated by a brass cylinder

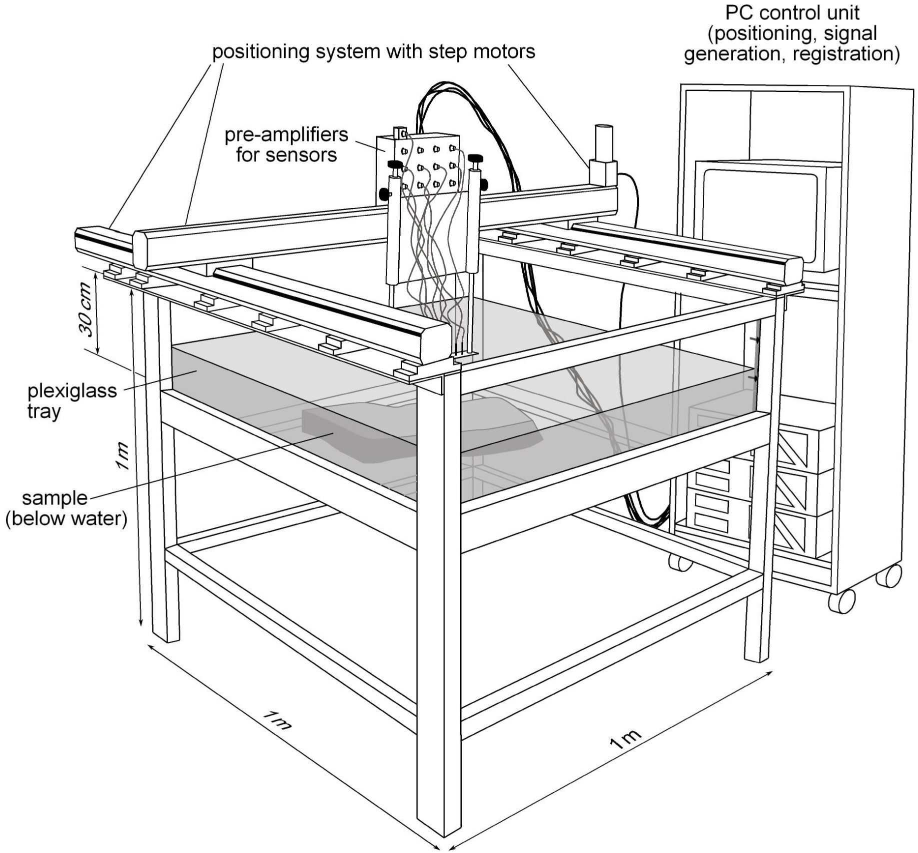

Fig. 1. Experimental device and setup of the mini-seismic system in the laboratory. The system consists of a seismic tank, a PC-driven control unit, a positioning system, and piezo-electric transducers (for technical details see also Table 1 and Figs. 2 and 3).

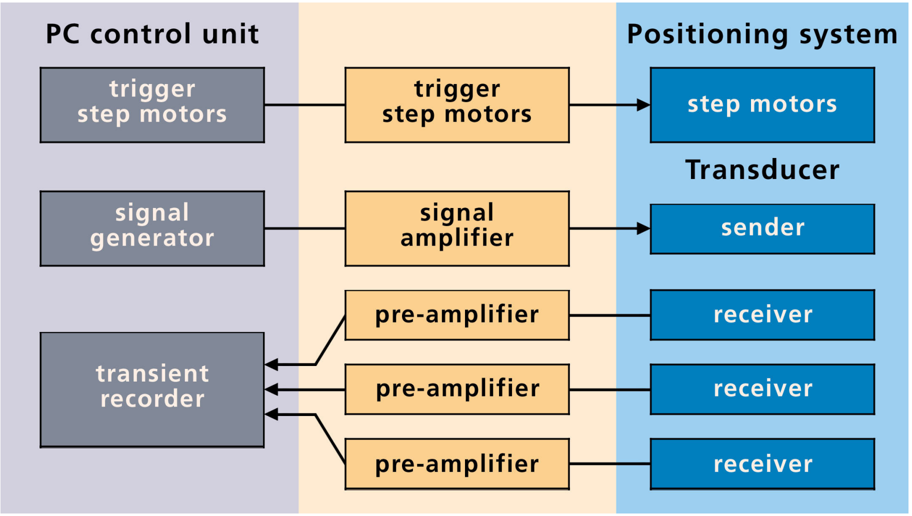

Fig. 2. Schematic illustration of the functions performed by the PC control unit for communication with the positioning system and the transducers.

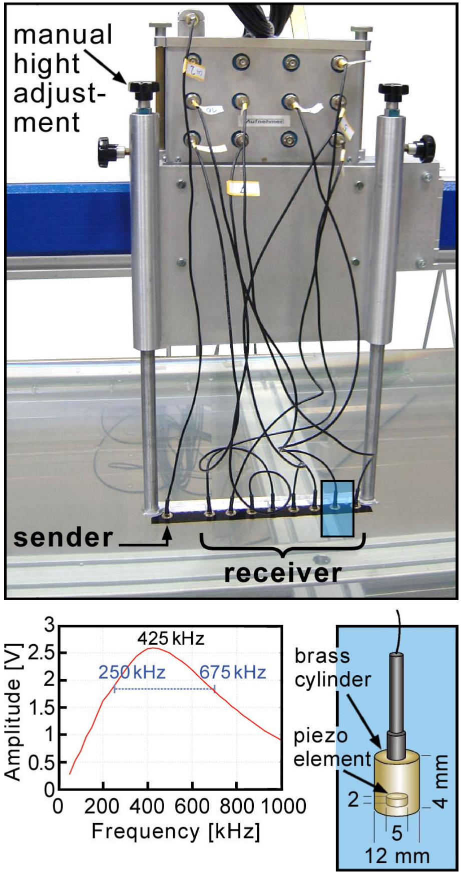

Fig. 3. Transducer array (top) and technical characteristics of the piezo-electric elements used (bottom).

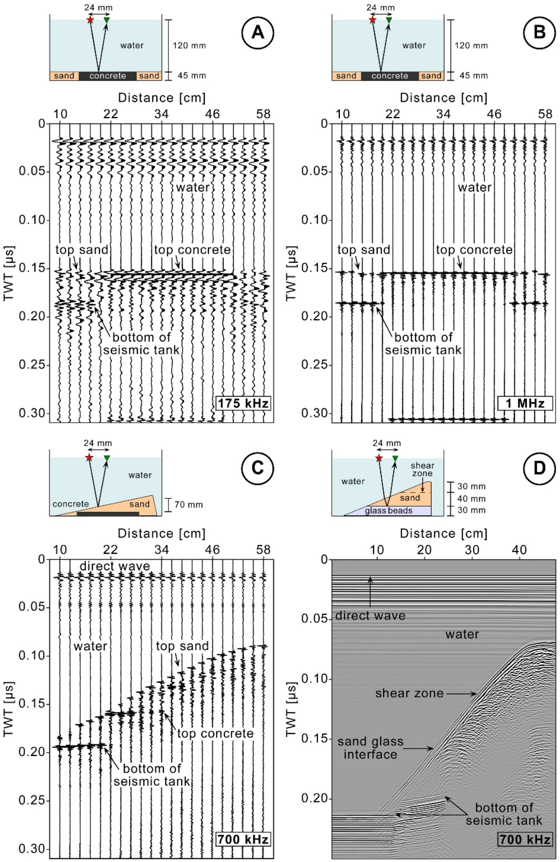

Fig. 4. Principle experiment geometries and resulting common-offset gathers from different test series acquired with the laboratory seismic system. **A, B** – flat reflector experiments testing different source frequencies; **C, D** – wedge experiments with different layer materials for attenuation and scattering analyses.

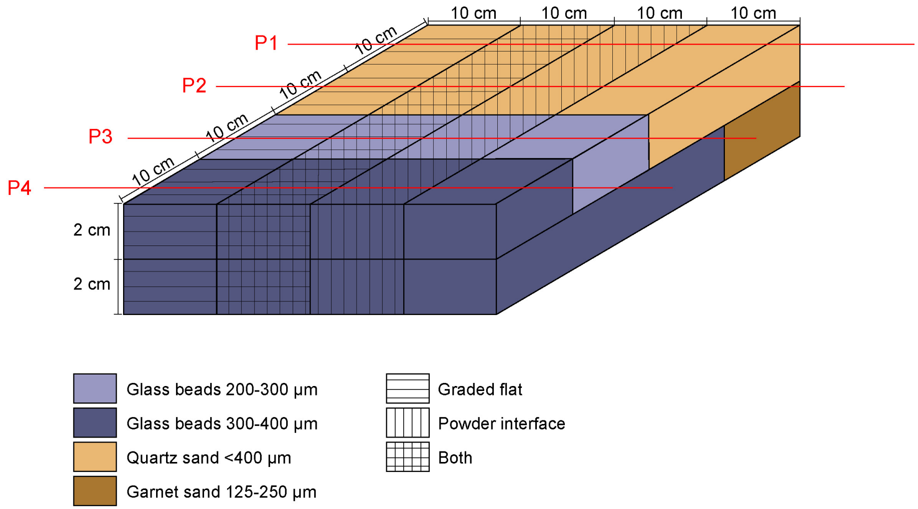

Fig. 5. Setup of the interface model to test seismic imaging properties of selected granular materials and of differently prepared interfaces. The lines labelled P1-P4 mark the locations of the seismic sections shown in Fig. 6.

Title Page
Abstract
Introduction
Conclusions
References
Tables
Figures
◀I
▶I
◀
▶
Back
Close
Full Screen / Esc
Printer-friendly Version
Interactive Discussion

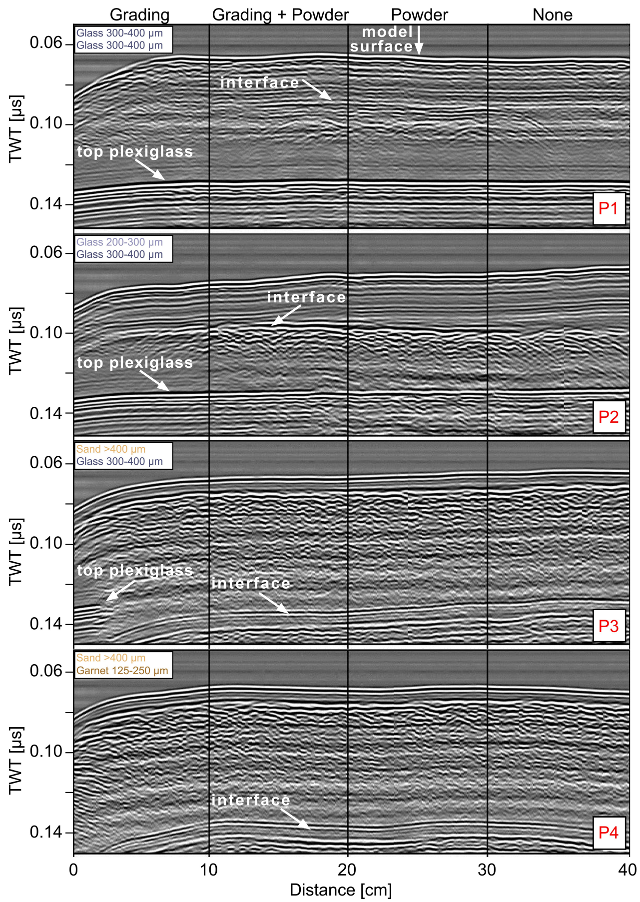

Fig. 6. Reflection seismic sections across the interface model located at lines P1-P4 given in Fig. 5. The interface is best imaged when it is prepared by grading and powder (P+Gr) as well as between well-rounded and well sorted glass beads (P3, P4).

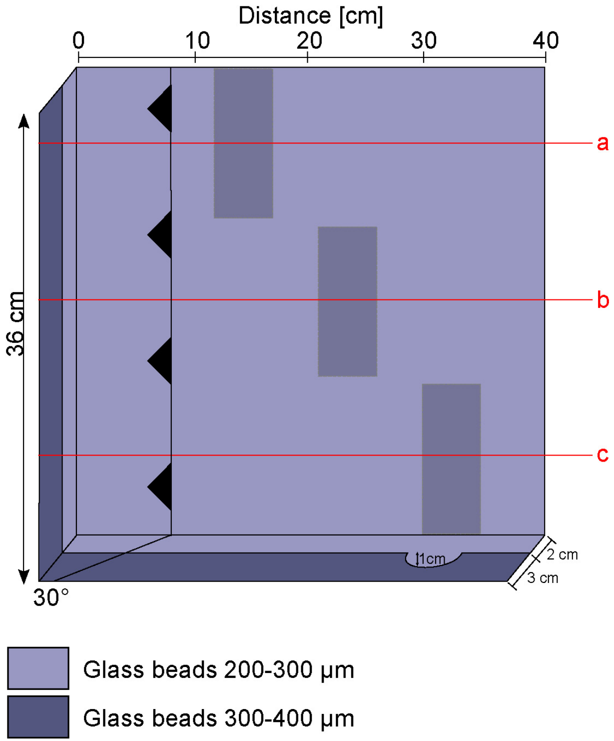

Fig. 7. Setup of the channel model consisting of two glass bead layers. While a shear zone of 30° dip angle is prepared close to the left side of the analogue model, a channel structure is distributed over three positions in the model. Lines **a–c** mark locations of the seismic sections shown in Fig. 8.

Title Page
Abstract | Introduction
Conclusions | References
Tables | Figures
◀◀ | ▶▶
◀ | ▶
Back | Close
Full Screen / Esc

Printer-friendly Version

Interactive Discussion

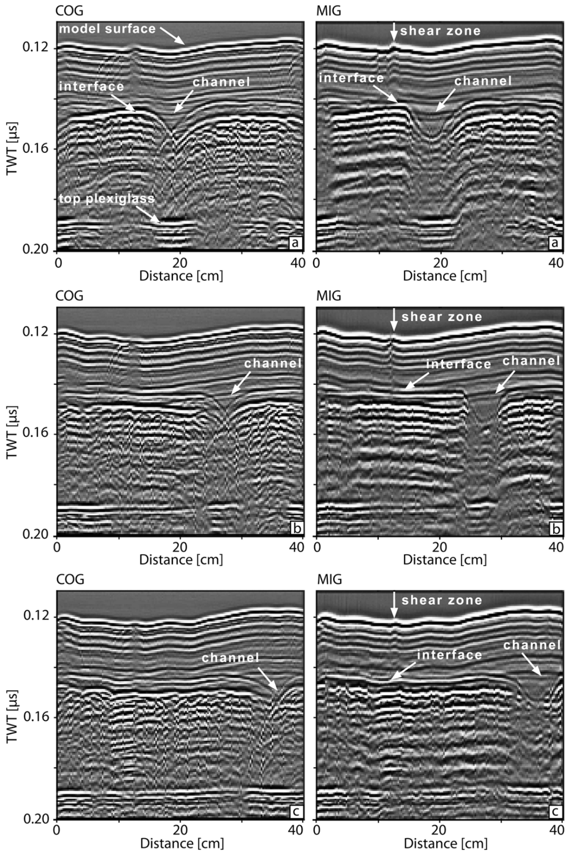

Fig. 8. Constant offset gathers (COG; left) and time-migrated sections (MIG, right) image the channel model at three different profile positions across the analogue model (cf. Fig. 7, profiles **a–c**). The distance between shear zones and channel structures varies, but in all sections these can be clearly imaged separately.